SUPPLEMENTAL METHODS

EXPOSURE DATING

To sample the shoreline we selected a site about 280 m west of the nearest inselberg (Jebel Hawaja; Figure 2) to reduce the possibility of slope wash reaching the sample site. Aerial images show slope wash halos around the inselbergs and a post-depositional alluvial fan 2 m thick flanking the inselberg and extending over the adjacent shoreline to at least 100 m. A 3 m trench (Section S2 of Williams et al. (2010)) was excavated using a bulldozer and 6 samples were collected at 0.5 m intervals down the pit wall. Field observations and particle size analysis at site S2 (Figure 2) show a decrease in gravel content and an increase in sand from the base upwards, consistent with lake retreat, a decrease in wave energy and final deposition of a sandy beach at the site. A well developed soil has subsequently formed on top of the shoreline sediment.

The granite was crushed and a coarse quartz concentrate was prepared using heavy liquids and magnetic separation. Only the coarse sand (>0.5 cm) and gravel fraction of the shoreline sediment was used for ^{10}Be analysis. We purified quartz and extracted ^{10}Be using standard methods (Barrows et al., 2001). The surface sample was run in duplicate. Isotopic ratios (^{10}Be/Be) were measured by accelerator mass spectrometry on the 14UD accelerator at the Australian National University.

To investigate the potential for sequential deposition of the shoreline and to quantify inheritance of cosmogenic nuclides in the sand and gravel, we used a profile dating approach. Prolonged exposure of a sediment column to cosmic rays produces a characteristic cosmogenic nuclide depth profile that is a function of the production rate of the nuclide, sediment density, the accumulation or erosion rate of the sediment, and inherited nuclides in the sediment from previous exposure at the sediment source. Ideal conditions for exposure

dating a profile are rapid deposition, an absence of post-depositional accumulation or erosion of the surface, and rapid erosion rates at the sediment source, which delivers a minimal inherited nuclide component. The setting of the Jebelein shoreline satisfies these suitability criteria. The ridge represents a high-energy depositional environment and therefore was deposited in a brief period of time. Second, there is no geomorphic evidence for widespread erosion of the surface in the form of gullying. Third, there appears to have been limited post-depositional accumulation of sediment on the surface. However, inheritance is likely to be significant because weathering rates are low on inselbergs in desert environments (e.g., Bierman and Caffee (2002)).

Cosmogenic nuclide production rates are a topic of active research and as yet no consensus has emerged as to a ^{10}Be production rate and a single scaling scheme that is globally applicable. The CRONUS calibration data set gives a ^{10}Be production rate by spallation of 4.49 ± 0.39 atom $g^{-1}a^{-1}$ at high latitude and sea level using the (Stone, 2000) scaling scheme (Balco et al., 2008). However, recent calibrations indicate that this rate is too high by at least 10% (Balco et al., 2009; Fenton et al., 2011; Kaplan et al., 2011; Putnam et al., 2010). In the absence of a regional production rate calibration, we used the North American regional production rate of Balco et al. (2009) which is at a similar elevation (<500 m) and within uncertainties is the same as the other recent Northern hemisphere calibration (Fenton et al., 2011). It also has a longer calibration exposure age incorporating more geomagnetic variability. To scale the production rates we use the scaling scheme of (Lifton et al., 2005). Barrows et al. (2013) have shown that the Lifton et al. (2005) scheme produced the best match between ^{10}Be and radiocarbon dates in New Zealand. The calculated ^{10}Be concentrations, ages and weathering rates are given in Supplemental Table 2.

To determine the exposure age for the profile, we updated the coefficients of the equations used in Granger and Smith (2000) for the ^{10}Be production rate of Balco et al.

(2009) from that of Stone (2000). Maximum likely inheritance on the gravel was determined by processing three samples from the top of the adjacent Jebel Hawaja. The morphology of the inselbergs at Jebelein, including exfoliation and solution pits, indicates a low long-term weathering rate.

The uppermost part of the section appears to be reworked. OSL dating of fine sand in the surface soil at a depth of 56 cm yielded an apparent age of 3.0-3.1 ka. Fine sand from 106 cm showed very high dispersion and had equivalent dose values at about 1.5 Gy and 120 Gy, corresponding to ages between 2.0 ka and 158 ka (Williams et al., 2010). Additionally a portable dolerite murhakah (lower grinding stone) was found within the soil after excavation, but from an unknown depth. The age of this grindstone is difficult to determine because their use extends from the upper Palaeolithic through to the recent. Dozens of grinding holes and thick camp site hearth deposits of charcoal and broken bone line the edges of nearby inselbergs adjacent to the Nile River and indicate an important site of Neolithic habitation during a time when grassland was more widespread, probably before 4,500 ^{14}C yr BP. We therefore consider it likely that the grindstone was incorporated into the profile during the mid Holocene and therefore the upper part of the sediment profile was probably reworked at this time. It is also possible that some slope wash from the inselberg has reached the site and lowered the mean ^{10}Be concentration of the surface sediment. For these reasons we chose to analyse the coarse sand and gravel which has a much lower potential for translocation both up and down the profile. Our logging showed that original bedding of the coarse clasts is intact below the surface of the soil (Fig. 2).

We used the CRONUS online calculator (Balco et al. 2008) to calculate the ^{10}Be production rate at the site. The exposure age (together with inheritance) was calculated from a least squares fit of a curve that is a sum of exponentials representing spallation, slow muon

capture and fast muons (Granger and Smith, 2000). Because the relative errors are similar on each sample, we did not weight the fit.

The density of the sediment varies through the profile and so it was not possible to determine an integrated mean density for use in the calculations. The density of sand and gravel mixtures ranges from 1.6-2.1 g/cm^3, so we chose a density of 1.9 g/cm^3. Variations of 0.1 g/cm^3 in density change the exposure age by ~2 %. A density of 2.7 g/cm^3 was used for the granite samples. The quoted uncertainties are 68% confidence limits incorporating all known sources of measurement error, and include fully propagated production rate errors.

OPTICALLY STIMULATED LUMINESCENCE

Seven samples were collected for optically stimulated luminescence (OSL) dating from channel sands and overlying sediments, and one sample was collected from the modern White Nile to assess the extent to which the OSL signal is reset at deposition in this environment. Samples were collected by inserting an opaque tube into the sediment. This was then sealed at both ends and wrapped in black plastic. In the laboratory the material from both ends of the tube, which would have been exposed to light, was scraped out and used for environmental dose rate measurements.

Samples were processed either at Aberystwyth University or at the University of Adelaide. The comparability of the two sets of analysis has previously been demonstrated (Macklin et al., 2013). Samples were prepared using similar procedures in both laboratories. Samples were initially treated with hydrochloric acid to digest carbonates and hydrogen peroxide to remove any small amounts of organic material. Grains in the ranges 180–212 μm (Aberystwyth) and 125-180 μm (Adelaide) were selected by dry sieving. Solutions of sodium polytungstate were used to isolate grains with a density between 2.62 and 2.70 g/cm^3. Grains were etched for 40 minutes in 40% hydrofluoric acid to remove feldspar and other non-quartz

material and to remove the outer 9 μm of the quartz grains. This eliminates the effect of alpha particle contribution to the irradiation of the grains. The material was then re-sieved to remove any remaining feldspar grains. All the laboratory procedures were carried out in subdued red light.

In Adelaide, uranium (U), thorium (Th) and potassium (K) concentrations were measured by Genalysis Laboratories, Perth, using Inductively Coupled Plasma Mass Spectroscopy (ICPMS) for U and Th, and Inductively Coupled Plasma Atomic Emission Spectrometry (ICPAES) for K. U and Th concentrations were also measured by thick source alpha counting (TSAC) in the Adelaide laboratory, and K concentrations by CSIRO laboratories, Adelaide, using X-ray fluorescence spectroscopy (XRS). The cosmic ray contribution was obtained using the relationship between cosmic ray penetration, depth and latitude determined by (Prescott and Hutton, 1994). The radionuclide concentrations obtained by the various methods were averaged, and the dose rate to be used in the age calculation, as well as the beta and gamma contributions to this dose rate, was determined using the AGE program of Grün (see Grün (2009)).

In Aberystwyth, beta dose rate was determined using a Risø beta counter (Bøtter-Jensen and Mejdahl, 1988), and the concentration of U, Th and K in the samples was determined using geochemical methods. For each sample, a finely milled sub-sample was fused using a sodium metaborate flux and put into solution. The resulting solutions were analysed using ICP-OES to determine the concentration of K and ICP-MS to determine the concentration of U and Th. The conversion factors of Adamiec and Aitken (1998) were then used to calculate the gamma dose rate. The cosmic ray contribution was obtained using the relationship between cosmic ray penetration, depth and latitude determined by Prescott and Hutton (1994). Water content of the material as received was measured by weighing, drying overnight at 180ºC, and re-weighing. A value of 5 ± 2% was used as the best estimate of the

water content during the period of burial for all samples except the sample from the modern White Nile where a value of 10 ± 5% was used (Note: an increase of 1% in the water content causes an increase of approximately 1% in the measured age of the sample). The results of these measurements, and the calculated dose rates, are given in Table S3.

Luminescence measurements for sample S10/5-2 were carried out at the University of Adelaide, and the other six samples including the surface sample were measured at the Aberystwyth Luminescence Research Laboratory (ALRL) at Aberystwyth University.

Luminescence measurements in Adelaide

In Adelaide luminescence measurements were made on small aliquots consisting of between about 50 to 100 grains in the 125-180 μm range. Pilot studies had indicated that this number of grains would enable individual differences between the aliquots to be detected, while still providing measurable luminescence. Luminescence measurements were carried out using a Risø TL/OSL-DA-20 reader. Radiation was applied using a calibrated $^{90}Sr/^{90}Y$ β source delivering a dose rate of 0.135 Gy/sec. Luminescence was stimulated using blue light-emitting diodes (wavelength 470 nm) and detected using an EMI 9235QB photomultiplier and Hoya U340 filter. The measurement procedure followed the single aliquot regeneration (SAR) protocol described by Murray and Wintle (2000). Four regeneration doses were used, selected on the basis of a pilot study, plus a zero dose point to test for recuperation, a repeat of the first dose to test for acceptable recycling and a second repeat of the first dose followed by exposure to infra-red radiation to test for the absence of feldspars (IR depletion test). 24 aliquots were run, and those having recycling ratios greater than 0.85, recuperation less than 0.15 and IR depletion ratio less than 0.15 were accepted for analysis. 23 out of the 24 aliquots passed the screening criteria. The equivalent dose D_e was determined for each aliquot by interpolation of its dose response (luminescence vs dose) curve. The equivalent dose is the

147 laboratory-applied dose that produces luminescence equal to that of the natural sample and is
148 hence equal to the total burial dose.

149 The individual D_e values showed a fairly well constrained distribution with six clearly
150 outlying high values. The D_e values were combined, omitting the outliers, using the central
151 age model (CAM) to derive a final D_e value for age calculation.

152 *Luminescence measurements in Aberystwyth*

153 In Aberystwyth luminescence measurements were made on aliquots containing ~500
154 grains of quartz between 180-211 μm in diameter. A Risø TL/OSL reader model TL-DA-15
155 was used for measurements. Blue LEDs (470Δ20 nm) were used for optical stimulation, and
156 the resulting OSL was detected using an EMI 9635QA photomultiplier fitted with 7.5mm of
157 Hoya U-340 filter. The resulting OSL signals showed a rapid initial decrease in intensity (Fig.
158 S1a) as would be expected from samples where the OSL signal is dominated by the fast
159 component. As in Adelaide, the SAR method was used, and typically 6 to 7 regeneration
160 doses were used to characterise the dose response curve and calculate the equivalent dose
161 (D_e) for each aliquot (Fig. S1b). Uncertainties on individual D_e values were determined using
162 the approach outlined in Duller (2007) which incorporates the uncertainty due to counting
163 statistics on each individual OSL decay curve, the uncertainty in the curve fitting procedure,
164 and also a 1.5% uncertainty associated with the Risø instruments used for these
165 measurements. Twenty-four replicate measurements of D_e were made for each sample. Data
166 was screened using standard acceptance criteria, including (1) a recycling ratio within 10% of
167 unity, (2) an IR depletion ratio (Duller, 2003) within 10% of unity, (3) a net OSL signal from
168 the test dose that is at least three times larger than the standard deviation of the background,
169 (4) a dose response curve that increases monotonically and (5) a natural signal (and
170 associated uncertainty) that intersects with the dose response curve. This screening removed
171 very few aliquots, with between 21 and 24 aliquots passing all of these criteria.

The modern sample from the White Nile (S11/WN1) gave an age of 0 ± 21 years, demonstrating that quartz is very effectively reset by exposure to daylight at the time of deposition in this environment. One of the limitations of luminescence dating is the impact of saturation of the OSL signal at high doses. The form of the dose response curve (Fig. S1b) is either a single saturating exponential, or the sum of two saturating exponential functions. As the radiation dose to which a sample is exposed increases, the rate of growth of the OSL signal decreases, until at some point there is negligible growth. Beyond this point it is not possible to resolve samples of different age. A number of the samples in this study have large D_e values (> 100 Gy, Table S4), but no more than 2 aliquots from 24 measured for each sample failed because the OSL signal was saturated. However, one feature of the samples with a high D_e (> 100 Gy) is that they tend to have dose distributions (Fig. S1c) with overdispersion values (25-30%) slightly higher than is normally encountered in younger samples, and this is thought to result from curvature of the dose response curve. There is no evidence that this overdispersion is related to incomplete resetting of the luminescence signal at deposition, and the age of 0 ± 21 years for the modern sample supports this. Therefore, the D_e values for each sample were combined using the central age model (CAM) to derive a final D_e value for age calculation. The equivalent doses, dose rates and ages for all the luminescence samples are summarised in Table S4.

LAKE RECONSTRUCTION

The SRTM90m digital elevation model (DEM) released by NASA has a 3 arc second horizontal resolution and a ~5 m vertical precision in this region, and was used to map the White Nile River valley in ARCGIS (Fig. 1). Palaeoshorelines are obvious in many areas and were mapped directly from the DEM. The height of the shoreline drops by ~5 m over a distance of 400 km, indicating a gradient of ~ 1:80,000. This is due to incomplete damming of the lake. Contours were generated at 395 m in the lower catchment and 400 m in the upper

197 catchment, which showed the best fit to the top of the shorelines. This allowed for the
198 shoreline of the entire lake to be extrapolated to where shorelines were absent. The area and
199 volume of the palaeolake were calculated in GIS by filling the valley to the appropriate
200 height, whilst taking into account the underlying topography.

201

SUPPLEMENTAL REFERENCES

Adamiec, G., and Aitken, M. J., 1998, Dose-rate conversion factors: update: Ancient TL v. 16, no. 2, p. 37-50.

Balco, G., Briner, J., Finkel, R. C., Rayburn, J. A., Ridge, J. C., and Schaefer, J. M., 2009, Regional beryllium-10 production rate calibration for late-glacial northeastern North America: Quaternary Geochronology, v. 4, no. 2, p. 93-107.

Balco, G., Stone, J. O., Lifton, N. A., and Dunai, T. J., 2008, A complete and easily accessible means of calculating surface exposure ages or erosion rates from 10Be and 26Al measurements: Quaternary Geochronology, v. 3, no. 3, p. 174-195.

Barrows, T. T., Stone, J. O., Fifield, L. K., and Cresswell, R. G., 2001, Late Pleistocene Glaciation of the Kosciuszko Massif, Snowy Mountains, Australia: Quaternary Research, v. 55, no. 2, p. 179-189.

Barrows, T. T., Almond, P., Rose, R., Keith Fifield, L., Mills, S. C., and Tims, S. G., 2013, Late Pleistocene glacial stratigraphy of the Kumara-Moana region, West Coast of South Island, New Zealand: Quaternary Science Reviews, v. 74, no. 0, p. 139-159.

Bierman, P. R., and Caffee, M., 2002, Cosmogenic exposure and erosion history of Australian bedrock landforms: Geological Society of America Bulletin, v. 114, no. 7, p. 787-803.

Bøtter-Jensen, L., and Mejdahl, V., 1988, Assessment of beta dose-rate using a GM multicounter system: International Journal of Radiation Applications and Instrumentation. Part D. Nuclear Tracks and Radiation Measurements, v. 14, no. 1–2, p. 187-191.

Duller, G. A. T., 2003, Distinguishing quartz and feldspar in single grain luminescence measurements: Radiation Measurements, v. 37, no. 2, p. 161-165.

-, 2007, Assessing the error on equivalent dose estimates derived from single aliquot regenerative dose measurements: Ancient TL v. 25, p. 15-24.

Fenton, C. R., Hermanns, R. L., Blikra, L. H., Kubik, P. W., Bryant, C., Niedermann, S., Meixner, A., and Goethals, M. M., 2011, Regional 10Be production rate calibration for the past 12 ka deduced from the radiocarbon-dated Grøtlandsura and Russenes rock avalanches at 69° N, Norway: Quaternary Geochronology, v. 6, no. 5, p. 437-452.

Granger, D. E., and Smith, A. L., 2000, Dating buried sediments using radioactive decay and muogenic production of 26Al and 10Be: Nuclear Instruments and Methods in Physics Research Section B: Beam Interactions with Materials and Atoms, v. 172, no. 1-4, p. 822-826.

Grün, R., 2009, The "Age" programme for the calculation of luminescence age estimates: Ancient TL v. 27, p. 45-46.

Kaplan, M. R., Strelin, J. A., Schaefer, J. M., Denton, G. H., Finkel, R. C., Schwartz, R., Putnam, A. E., Vandergoes, M. J., Goehring, B. M., and Travis, S. G., 2011, In-situ cosmogenic ^{10}Be production rate at Lago Argentino, Patagonia: Implications for late-glacial climate chronology: Earth and Planetary Science Letters, v. 309, no. 1â€“2, p. 21-32.

Lifton, N. A., Bieber, J. W., Clem, J. M., Duldig, M. L., Evenson, P., Humble, J. E., and Pyle, R., 2005, Addressing solar modulation and long-term uncertainties in scaling secondary cosmic rays for in situ cosmogenic nuclide applications: Earth and Planetary Science Letters, v. 239, no. 1-2, p. 140-161.

Macklin, M. G., Woodward, J. C., Welsby, D. A., Duller, G. A. T., Williams, F. M., and Williams, M. A. J., 2013, Reach-scale river dynamics moderate the impact of rapid

Holocene climate change on floodwater farming in the desert Nile: Geology, v. 41, no. 6, p. 695-698.

Murray, A. S., and Wintle, A. G., 2000, Luminescence dating of quartz using an improved single-aliquot regenerative-dose protocol: Radiation Measurements, v. 32, no. 1, p. 57-73.

Prescott, J. R., and Hutton, J. T., 1994, Cosmic ray contributions to dose rates for luminescence and ESR dating: Large depths and long-term time variations: Radiation Measurements, v. 23, no. 2–3, p. 497-500.

Putnam, A. E., Schaefer, J. M., Barrell, D. J. A., Vandergoes, M., Denton, G. H., Kaplan, M. R., Finkel, R. C., Schwartz, R., Goehring, B. M., and Kelley, S. E., 2010, In situ cosmogenic ^{10}Be production-rate calibration from the Southern Alps, New Zealand: Quaternary Geochronology, v. 5, no. 4, p. 392-409.

Stone, J. O., 2000, Air pressure and cosmogenic isotope production: Journal of Geophysical Research, v. 105, p. 23,753-723,759.

Williams, M. A. J., Williams, F. M., Duller, G. A. T., Munro, R. N., El Tom, O. A. M., Barrows, T. T., Macklin, M., Woodward, J., Talbot, M. R., Haberlah, D., and Fluin, J., 2010, Late Quaternary floods and droughts in the Nile valley, Sudan: new evidence from optically stimulated luminescence and AMS radiocarbon dating: Quaternary Science Reviews, v. 29, no. 9-10, p. 1116-1137.

Supplemental Table S1. Site data

Sample	Longitude (°N)	Latitude (°E)	Altitude (m)	Horizon correction	Thickness/depth (cm)[1]	Muon production rate (atoms g^{-1} yr^{-1})
Jebel Hawaja						
JEB-01	12° 35' 3.3"	32° 50' 8.1"	426	1	3.0	0.210
JEB-02	12° 35' 3.6"	32° 50' 7.1"	427	1	2.5	0.210
JEB-03	12° 35' 4.0"	32° 50' 6.8"	425	1	3.0	0.210
Jebelein shoreline						
JEB-S06	12° 35' 7.5"	32° 49' 55.9"	402	1	2.5	0.209
JEB-S05	12° 35' 7.5"	32° 49' 55.9"		1	55	
JEB-S04	12° 35' 7.5"	32° 49' 55.9"		1	105	
JEB-S03	12° 35' 7.5"	32° 49' 55.9"		1	165	
JEB-S02	12° 35' 7.5"	32° 49' 55.9"		1	205	
JEB-S01	12° 35' 7.5"	32° 49' 55.9"		1	275	

1. Samples at Jebel Hawaja were exposed at the surface. Samples at the Jebelein shoreline are shown in depth below the surface (± 5 cm)

Supplemental Table S2. ^{10}Be results

Sample	Lab code	Production Rate (atoms g^{-1} yr^{-1}) Muons	$[^{10}Be]_c$ ($x10^5$ g^{-1})	Weathering rate (m/Ma)[1]
Jebel Hawaja				
JEB-01	ANU-M392-02		25.2 ± 1.70	0.73 ± 0.12
JEB-02	ANU-M392-03		9.90 ± 0.70	2.64 ± 0.33
JEB-03	ANU-M392-04		6.26 ± 0.46	4.62 ± 0.54
Section S2				
JEB-S2-06a	ANU-M392-05		5.01 ± 0.21	
JEB-S2-06b	ANU-M430-11		5.56 ± 0.26	
JEB-S2-05	ANU-M430-10		5.58 ± 0.24	
JEB-S2-04	ANU-M430-09		4.17 ± 0.18	
JEB-S2-03	ANU-M430-08		3.72 ± 0.18	
JEB-S2-02	ANU-M430-07		3.88 ± 0.18	
JEB-S2-01	ANU-M392-06		3.30 ± 0.14	

Data are normalised to NIST SRM 4325 assuming $^{10}Be/^{9}Be = 2.79 \times 10^{-11}$.
Carrier $^{10}Be/^{9}Be = <1 \times 10^{-15}$. ^{10}Be decay constant = 4.998×10^{-7} yr^{-1}.
Sample density for granite = 2.7 g cm^{-3}
1. Calculated using CRONUS online calculator and Wrapper script: 2.2, Main calculator: 2.1, Objective function: 2.0, Constants: 2.2.1, and Muons: 1.1 versions

Supplemental Table S3. Sample data for optical ages

Site	Sample	Depth (m)	Aliquots	H_2O %	K (%)	U (ppm)	Th (ppm)
B	S11/1-1	1.20 ± 0.10	22	5 ± 2	1.10 ± 0.06	0.76 ± 0.04	2.59 ± 0.13
B	S11/1-2	1.50 ± 0.20	23	5 ± 2	1.09 ± 0.06	0.67 ± 0.03	2.00 ± 0.10
B	S11/1-3	2.35 ± 0.50	21	5 ± 2	0.97 ± 0.05	0.67 ± 0.03	1.82 ± 0.09
C	S10/5-2	1.10 ± 0.10	22	5 ± 2	0.87 ± 0.03	1.03 ± 0.07	3.72 ± 0.24
C	S10/5-3	1.50 ± 0.10	21	5 ± 2	0.90 ± 0.05	0.64 ± 0.03	1.78 ± 0.09
C	S10/5-4	1.65 ± 0.10	24	5 ± 2	0.92 ± 0.05	0.67 ± 0.03	1.33 ± 0.07
D	S11/3-1	0.80 ± 0.50	22	5 ± 2	0.93 ± 0.05	1.03 ± 0.05	1.14 ± 0.06
E	S11/WN1	0.00 ± 0.10	24	10 ± 5	0.97 ± 0.05	0.56 ± 0.03	0.78 ± 0.04

Supplemental Table S4. Dose and dose rates for optical ages

Site	Sample	External β dose 'wet' (Gy/ka)	External γ dose 'wet' (Gy/ka)	Cosmic dose (Gy/ka)	Total dose rate (Gy/ka)	Equivalent dose (Gy)	Age (ka)
B	S11/1-1	0.99 ± 0.04	0.45 ± 0.02	0.18 ± 0.02	1.62 ± 0.05	112 ± 6.2	69 ± 4
B	S11/1-2	0.90 ± 0.04	0.41 ± 0.02	0.17 ± 0.02	1.48 ± 0.04	130 ± 6.2	88 ± 5
B	S11/1-3	0.83 ± 0.04	0.38 ± 0.02	0.16 ± 0.04	1.36 ± 0.06	140 ± 10	103 ± 9
C	S10/5-2	0.79 ± 0.05	0.48 ± 0.05	0.19 ± 0.02	1.47 ± 0.04	15.3± 1.5	10.4 ± 1.1
C	S10/5-3	0.71 ± 0.03	0.36 ± 0.02	0.17 ± 0.02	1.24 ± 0.03	141 ± 9.6	113 ± 8
C	S10/5-4	0.85 ± 0.04	0.34 ± 0.01	0.17 ± 0.02	1.36 ± 0.04	156 ± 13	115 ± 10
D	S11/3-1	0.80 ± 0.03	0.38 ± 0.02	0.19 ± 0.04	1.36 ± 0.05	142 ± 7.0	104 ± 6
E	S11/WN1	0.65 ± 0.04	0.30 ± 0.02	0.30 ± 0.03	1.25 ± 0.06	0.00 ± 0.02	0.00 ± 0.02

Note:
Grain Size 180-211μm for all samples except S10/5-2 for which grains 150-180μm in diameter were used.

Figure S1: Luminescence characteristics of a typical sample (S10/5-3). (a) Natural OSL decay curve. Note the log scale on the y-axis, (b) dose response curve and (c) radial plot showing the distribution of D_e values.

(a)

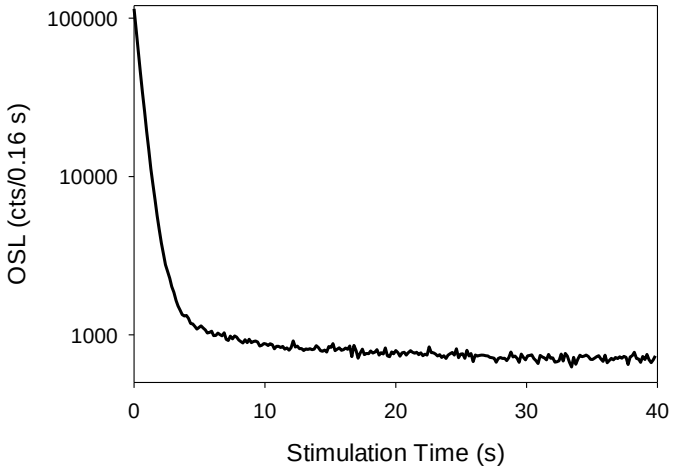

(b)

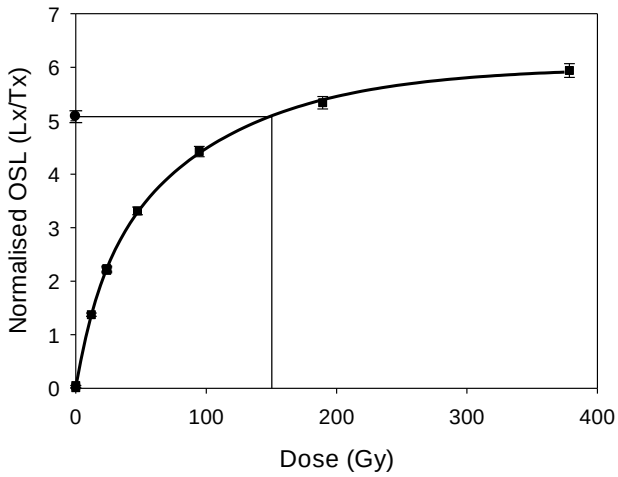

(c)